Forward Modeling of the Internal Layers in Radio Echo Sounding Using Electrical and Density Measurements from Ice Cores

William D. Miners,*,† Arne Hildebrand,‡ Sebastian Gerland,§,¶ Norbert Blindow,‡ Daniel Steinhage,‡,# and Eric W. Wolff†

British Antarctic Survey, High Cross, Madingley Road, Cambridge, CB3 0ET UK, Institut für Geophysik, Forschungsstelle für Physikalische Glaziologie, Westfälische Wilhelms-Universität Münster, D-48149 Münster, Germany, and Alfred-Wegener-Institut für Polar-und Meeresforschung, Postfach 120161, D-27515 Bremerhaven, Germany

Received: October 11, 1996; In Final Form: May 8, 1997[⊗]

The measured density and conductivity of a 181 m ice core are used to calculate a profile of complex reflection coefficients. It is confirmed that the amplitude reflection coefficients due to the conductivity variations are negligible in comparison to the amplitude reflection coefficients due to the density variations. Using the magnitudes of these reflection coefficients we obtain a profile of the expected power being returned to the surface. The modeled power return is compared with the results of a short pulse electromagnetic reflection survey near the drill site. We also convolve the profile of complex reflection coefficients with a depth invariant input wavelet to produce a synthetic radargram for the top part of the ice sheet. The phase change given to wavelets reflecting from the conductivity variations has a negligible effect on the synthetic radargram. Using this simple model we are unable to match the positions of the internal layers in the synthetic radargram with those in the reflection survey.

1. Introduction

When glaciologists carry out radio echo sounding (RES) over polar ice sheets, reflections occur from the bedrock and from layers inside the ice column.[1,2] There is still uncertainty as to the interpretation of these reflections from layers inside the ice column. Sometimes they have been linked to discrete layers in the ice such as volcanic horizons.[3,4] Yet it is also known that if the characteristics of the transmitted wavelet are altered, then the appearance of the internal reflections changes.[5] The transmitted wavelet will be reflected at any change in the complex permittivity of the ice column. The complex permittivity of the ice is controlled by the density, temperature, fabric orientation, chemical impurities, and the sizes and shapes of bubbles.[6−14]

The present consensus is that in the top few hundred meters of an ice sheet the permittivity variations are dominated by the changing density. In those parts of the echo where no single strong reflection dominates, the echo received at the surface consists of the interference between many weak wavelets reflecting from small changes in the permittivity.[7] The interference of wavelets depends on their shape and their magnitude. The reflected wavelets will have a different shape from the incident wavelet after reflecting from a boundary with a complex reflection coefficient.[15] Previous studies of this interference were hampered by the poor resolution of the ice core data used[15] or by not having access to a RES survey.[12] In this paper we have ice core data at centimeter resolution and a high-resolution, short pulse RES record for comparison.

* Author to whom correspondence should be addressed: E-mail, w.miners@bas.ac.uk.
† British Antarctic Survey.
‡ Universität Münster.
§ Alfred-Wegener-Institut.
¶ Present address: Norwegian Polar Institute, Storgata 25A, N-9008, Tromsø, Norway.
# Present address: Alfred-Wegener-Institut, Germany.
⊗ Abstract published in *Advance ACS Abstracts,* July, 1, 1997.

2. The Radar Survey

The electromagnetic reflection system used was that of the Forschungsstelle für Physikalische Glaziologie,[16] which transmitted a short pulse of center frequency 30 MHz (f_{cent}). The trace being used for this paper was recorded about 100 m from the drill site with a separation of 10 m between the transmitter and receiver. The returning signal was sampled every 1.7 ns. The data were processed in six steps: removal of the air wave (which dominates over the reflected wave for the first 300 ns of the recording), normal moveout correction, resample to model resolution of 0.1 ns (using cubic spline interpolation), bulk amplitude shift to remove the zero error at the start, 10 MHz high-pass filter, and true amplitude correction using the second power of the time.

3. The Ice Core Data

This paper uses data from a 181 m long ice core drilled at S79°36.85′ W045°43.46′ which is 5 km to the south of Thyssenhöhe, the southern dome of Berkner Island, Antarctica.[17,18] The density was used to calculate the real component of the relative permittivity (ϵ_r'), and the conductivity was used to calculate the imaginary component of the relative permittivity (ϵ_r'').

The density (Figure 1a) was derived from measurements, taken in the cold laboratory at the Alfred-Wegener-Institut, of the attenuation of a 2 mm wide beam of γ-rays from a cesium isotope specimen.[19] The ice core was moved through the γ-ray beam by a stepping motor in increments of 3 mm. The accuracy of the values used was ±2%.[20] The real relative permittivity was determined from the density using empirical eq 1:[21]

$$\epsilon_r' = (1 + 0.845\rho)^2 \quad (1)$$

ρ is the specific gravity. The conductivity was determined at the drill site in a subsurface chamber by dielectric profiling (DEP).[22] The DEP method[23] measures conductance and ca-

S1089-5647(96)03218-X CCC: $14.00

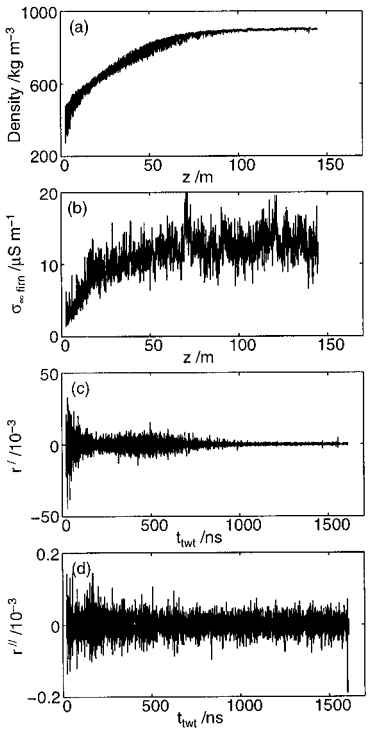

Figure 1. Properties for the top of the ice sheet: (a) the density (kg m^{-3}), (b) the calculated firn conductivity (μS m^{-1}), (c) the real component of the amplitude reflection coefficient (r′), (d) the imaginary component of the amplitude reflection coefficient (r″).

pacitance at one or more frequencies and was used on this core at a single frequency of 50 kHz, with a 15 mm wide top electrode, sampling every 10 mm. From the measured capacitance without the ice (C_{air}) and the measured conductance with the ice (G_{ice}) the conductivity (σ) was calculated using eq 2:

$$\sigma_{firn} = \frac{\epsilon_0 G_{ice}}{C_{air}} \tag{2}$$

ϵ_0 is the permittivity of vacuum 8.854×10^{-12} F m^{-1}. It has previously been found[24] that 50 kHz is sufficiently far above the main relaxation frequency of ice for the calculated 50 kHz conductivity to be in good agreement with the high-frequency limit of the conductivity of ice (σ_∞). The σ_∞ is controlled mainly by the density, temperature and the chemical content of the ice.[25]

The conductivity of the core measured in the subsurface chamber was converted into the expected conductivity at depth by a calculation using the temperatures in the two locations. The temperature in the upper part of the ice sheet was measured by lowering a series of thermistors down the borehole at the end of the drilling.[18] There were three steps in the conversion of the conductivity. First the conductivity was increased from that measured in the firn to that expected in solid ice using eq 3:[26]

$$\sigma_{\infty ice} = \frac{\sigma_{\infty firn}}{v(0.68 + 0.32\, v)^3} \tag{3}$$

v is the volume proportion of the firn, which can be approximated as the ratio of the density of the firn to that of solid ice. The second step was the temperature conversion using an Arrhenius relation,[27,28] using activation energies for the pure solid ice of 0.5 eV and the average for acid and salt of 0.22 eV. The final step was the reversal of the first, scaling back from the conductivity of solid ice to the conductivity of the firn. The accuracy of the final conductivity (Figure 1b) is estimated to be ±15%. The conductivity is used to give the imaginary relative permittivity by using eq 4:

$$\epsilon_r'' = \frac{\sigma_{\infty firn}}{2\pi f_{cent} \epsilon_0} \tag{4}$$

4. The Reflection Profile

To convert the complex permittivity profile from a function of depth (z) into a function of two way travel time (t_{twt}), a velocity profile was needed. For the accuracy of this model it was sufficient to use a nondispersive phase velocity(v_{ph}) that was a function of only the real permittivity, see eq 5:

$$v_{ph} = \frac{c}{\sqrt{\epsilon_r'}} \tag{5}$$

where c is the speed of electromagnetic waves in a vacuum. If the imaginary component of the permittivity were included in a full expression for the phase velocity,[6] then the t_{twt} for a wavelet to the bottom of the model was only 1 ps slower. The profile of permittivity as a function of t_{twt} was then resampled, using linear interpolation, so that the data points were every 0.1 ns. These equally spaced measurements in time (given the subscript i) are necessary for the eventual convolution with a wavelet sampled at the same resolution. The complex impedance (Z_i) of each of these new layers is given by eq 6:

$$Z_i = \left(\frac{\mu_0}{\epsilon_0 (\epsilon_{ri}' - j\epsilon_{ri}'')} \right)^{1/2} \tag{6}$$

where μ_0 is the permeability of vacuum $4\pi \times 10^{-7}$ H m^{-1}. The amplitude reflection coefficient (r) between these layers is given by eq 7:

$$r = \frac{Z_{i-1} - Z_i}{Z_{i-1} + Z_i} \tag{7}$$

In Figure 1c,d the real and imaginary components of the amplitude reflection coefficients are displayed.

5. Comparing the Model and the RES Trace

In each of the next two sections a different aspect of the output from the model is compared with the RES trace.

5.1. Comparing the Decay in the Received Power. Using the initial peak in the RES trace as an indication of the transmitted power (P_T), the returned fraction of the power was calculated. This is displayed as curve a in Figure 2. A similar fraction was calculated from the model profile of the amplitude reflection coefficients using the radar eq 8:[2]

$$\frac{P_R}{P_T} = \frac{G_t A_r q R}{4\pi [2z]^2 L} \tag{8}$$

R is the power reflection coefficient (equivalent to r^2). L includes two terms: firstly, the absorption of energy in each layer crossed by the wavelet as it travels to depth z then back to the surface, secondly, the transmission loss at each boundary crossed. The unknown quantities are the gain of the antenna (G_t), the effective area of the receiving antenna (A_r), and the refraction gain (q). These terms determine the size of the gap between curves a and b in Figure 2.

5.2. Comparing the Positions of the Internal Reflections. A normalized, depth invariant, real input wavelet was convolved, in the frequency domain, with each boundary in the reflection

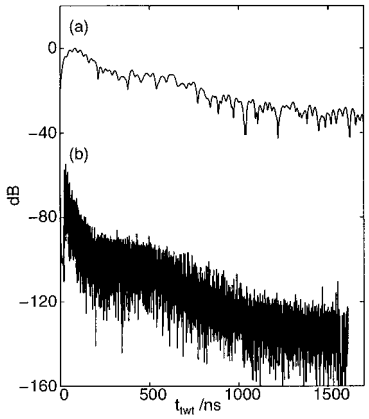

Figure 2. (a) The decibel ratio from the RES trace $\{10 \log_{10}(P_r P_t)\}$. (b) The decibel ratio from the model $\{10 \log_{10}(R/(16\pi r^2 L))\}$. The difference in the two curves is the term $10 \log_{10}(G_t A_r q)$.

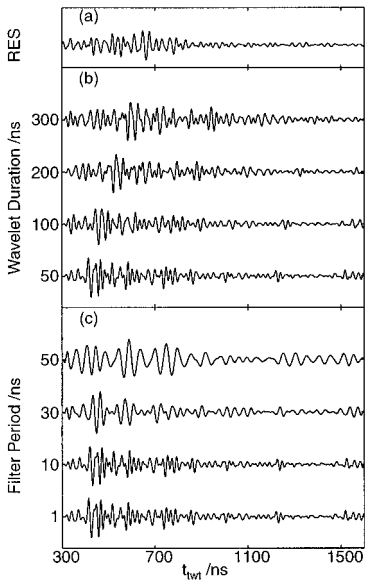

Figure 3. Amplitude profiles, after correction for spherical spreading, for the top of the ice sheet: (a) the RES trace, (b) radargrams using different length wavelets, (c) radargrams after smoothing the profile of two way travel time, permittivity. The smoothing was done with a low-pass Butterworth filter of order 6, the ordinate showing the time period of the shoulder frequency of the filter. The wavelet used in the convolution was 50 ns long.

profile.[15] The resulting synthetic radargram was then filtered to give it the same frequency content as the processed RES trace (10−70 MHz). As no signature wavelet was available for the RES, we used either an idealized Ricker wavelet[29] centered on f_{cent}, or extracted a wavelet from the RES. The extraction was done using a "cut-and-try" procedure similar to the early work on synthetic seismograms[30] using a symmetrical Gaussian envelope to extract part of the processed RES trace.

Despite experimenting with many different input wavelets, no similarity could be obtained between the internal layers in the synthetic radargram and the RES trace. These experiments therefore developed into an investigation of the performance of the model. Altering the ice core data, such as setting the conductivity to a constant value of 20 μS m^{-1}, made no noticeable change to the synthetic radargram. However, the model is sensitive to changes in the density; this was observed by applying a low-pass filter to remove the high-frequency features in the real permittivity. Figure 3c shows that the trace produced by the model starts to alter once features larger then 20 ns are smoothed out.

The influence of the input wavelet has been considered in previous work.[12] Where it was found that a shorter duration wavelet (Figure 3b) gave a greater resolution, a lower magnitude of response and caused the peaks in the radargram to shift up the trace. In this model the shift of the peaks was a result of the Gaussian envelope used to extract the wavelet.

6. Discussion

The value of the real reflection coefficients divided by the imaginary reflection coefficients has a modal value of 39.8 in the top 200 ns of the model and a modal value of 19.9 in the bottom 200 ns of the model. This is one example of the greater influence of the density variations near the surface and how the influence of the density variations starts to decrease with depth.

When convolving the profile of reflection coefficients with input wavelets, the effect of the conductivity profile, both in its contribution to the amplitude reflection coefficients and its phase altering ability, was negligible at these shallow depths. However, it is likely that the reflections seen in deeper ice may be due, in some cases, to discrete conductivity changes. For instance, the strong change in conductivity at the Holocene−Wisconsin boundary in Greenland[31] could be expected to produce a significant reflection.

Despite trying a variety of input wavelet shapes and lengths no satisfactory match was found between the positions of the internal layers in the synthetic radargram and the RES trace. This may be due to data deficiencies, such as the 100 m separation in the position of the ice core and the RES survey, or there may exist a better input wavelet. It is clear from Figure 3b that the nature of the wavelet can play a dominant role in the pattern of the reflections observed. So the search for the "best fit" wavelet is part of the continuing research.

A future model will probably need to consider the changes in the shape of the wavelet as it propagates through the ice. It may also be necessary to model the offset source and receiver instead of correcting the RES to vertical. Finally, we intend to test this model on ice core data from deeper ice where the effect of the offset source and receiver will be less. Also in deeper ice the use of a depth invariant wavelet (the far field signature of the radio echo system) may be more realistic.

Acknowledgment. We thank everybody who helped with the work on Berkner Island and provided useful comments on the manuscript: R. Mulvaney, H. Oerter, D. Peel, C. Doake, C. Lukait, M. Nolting, F. Töppe, E. Pasteur, U. Weigel, and S. Garrod.

References and Notes

(1) Robin, G. de Q.; Evans, S.; Bailey, J. T. *Philos. Trans. R. Soc. London, Ser A.* **1969**, *265*, 1166.
(2) Bogorodsky, V. V.; Bentley, C. R.; Gudmandsen, P. E. *Radioglaciology*; Reidel: Dordrecht, 1985.
(3) Hammer, C. U. *J. Glaciol.* **1980**, *25*, 93.
(4) Millar, D. H. M. *Nature* **1981**, 292.
(5) Millar, D. H. M. PhD Thesis, University of Cambridge, **1981**.
(6) Ewen Smith, B. M.; Evans, S. *J. Glaciol.* **1972**, *11*, 61.
(7) Harrison, C. H. *J. Glaciol.* **1973**, *12*, 66.
(8) Paren, J. G.; Robin, G. de Q. *J. Glaciol.* **1975**, *14*, 71.
(9) Gudmandsen, P. *J. Glaciol.* **1975**, *15*, 73.
(10) Clough, J. W. *J. Glaciol.* **1977**, *18*, 78.
(11) Ackley, S. F.; Keliher, T. E. *J. Geophys. Res.* **1979**, *84*, B10.
(12) Moore, J. C. *Ann. Glaciol.* **1988**, 11.
(13) Fujita, S.; Mae, S. *Ann. Glaciol.* **1993**, 17.
(14) Fujita, S.; Mae, S. *Ann. Glaciol.* **1994**, 20.
(15) Blindow, N. *Filchner Ronne Ice Shelf Programme. Report No. 8; Alfred-Wegener-Institute for Polar and Marine Research: Bremerhaven,* 1994.

(16) Steinhage, D.; Blindow, N. *Filchner Ronne Ice Shelf Programme. Report No. 9; Alfred-Wegener-Institute for Polar and Marine Research, Bremerhaven,* 1995.
(17) Jokat, W.; Oerter, H. *Berichte zur Polarforschung. Report No. 219; Alfred-Wegener-Institute for Polar and Marine Research: Bremerhaven,* 1997.
(18) Mulvaney, R. *Filchner Ronne Ice Shelf Programme. Report No. 9; Alfred-Wegener-Institute for Polar and Marine Research*: *Bremerhaven,* 1995.
(19) Gerland, S.; Kipfstuhl, S.; Graf, W.; Minikin, A. *Filchner Ronne Ice Shelf Programme. Report No. 8; Alfred-Wegener-Institute for Polar and Marine Research: Bremerhaven,* 1994.
(20) Gerland, S.; Oerter, H.; Kipfstuhl, J.; Wilhelms, F.; Frenzel, A.; Miners, W. D.; Mulvaney, R.; Peel, D. *Filchner Ronne Ice Shelf Programme. Report No. 10; Alfred-Wegener-Institute for Polar and Marine Research: Bremerhaven,* 1996.
(21) Kovacs, A.; Gow, A. J.; Morey, R. M. *Cold Reg. Sci. Technol.* **1995**, *23*, 3.
(22) Miners, W. D.; Mulvaney, R. *Filchner Ronne Ice Shelf Programme. Report No. 9; Alfred-Wegener-Institute for Polar and Marine Research: Bremerhaven,* 1995.
(23) Moore, J. C.; Paren, J. G. *J. Phys.* **1987**, *48* (Mar Suppl. 3), C1.
(24) Moore, J. C. *J. Glaciol.* **1993**, *39*, 132.
(25) Wolff, E. W.; Miners, W. D.; Moore, J. C.; Paren, J. G. Proceedings of the International Symposium on the Physics and Chemistry of Ice. *J. Phys. Chem*. In Press.
(26) Glen, J. W.; Paren, J. G. *J. Glaciol.* **1975**, *15*, 73.
(27) Hobbs, P. V. *Ice Physics*; Clarendon Press: Oxford, 1974; Chapter 2.
(28) Moore, J. C., Wolff, E. W.; Clausen, H. B.; Hammer, C. U.; Legrand, M. R.; Fuhrer, K. *Geophys. Res. Lett.*, **1994**, 21.
(29) Ricker N. *Geophysics* **1953**, 18.
(30) Peterson, R. A.; Fillipone, W. R.; Coker, F. B. *Geophysics* **1955**, 20.
(31) Wolff, E. W.; Moore J. C.; Clausen, H. B.; Hammer, C. U.; Kipfstuhl, J.; Fuhrer, K. *J. Geophys. Res.* **1995**, *100*, D8.